2019

Development of a variable stiffness magnetorheological damper with self-powered generation capability

Xiaojing Zhu
University of Wollongong, xz979@uowmail.edu.au

Lei Deng
University of Wollongong, ld530@uowmail.edu.au

Shuaishuai Sun
University of Wollongong, ssun@uow.edu.au

Tianhong Yan
China Jiliang University, thyan@163.com

Jianqiang Yu
Chongqing University, University of Wollongong

See next page for additional authors

Development of a variable stiffness magnetorheological damper with self-powered generation capability

Abstract

This article reports a compact stiffness controllable magnetorheological damper with a self-powered capacity. First, the structure, working mechanism, and analysis of the damper are presented. After the prototype of the magnetorheological damper, experimental tests were conducted to evaluate its variable stiffness feature and self-powered generation capability using a hydraulic Instron test system. The testing results demonstrate that its stiffness variation range can reach 70.4% when the applied current increases from 0 to 2 A. The energy generating capability of the magnetorheological damper was also evaluated using the Instron testing system under a harmonic excitation with 0.15 Hz frequency and 30 mm displacement. The testing results illustrate that the self-powered generation component can generate 2.595 W effective power, which is enough to control the magnetorheological component of the damper. The successful development, theoretical analysis, and experimental testing of this new variable stiffness self-powered magnetorheological damper make the concept of energy-free variable stiffness magnetorheological damper feasible.

Disciplines

Engineering | Science and Technology Studies

Publication Details

Zhu, X., Deng, L., Sun, S., Yan, T., Yu, J., Ma, Z. & Li, W. (2019). Development of a variable stiffness magnetorheological damper with self-powered generation capability. Journal of Intelligent Material Systems and Structures, Online First 1-11.

Authors

Xiaojing Zhu, Lei Deng, Shuaishuai Sun, Tianhong Yan, Jianqiang Yu, Zisu Ma, and Weihua Li

Published as:
Zhu, X., Deng, L., Sun, S., Yan, T., Yu, J., Ma, Z. & Li, W. (2019). Development of a variable stiffness magnetorheological damper with self-powered generation capability. *Journal of Intelligent Material Systems and Structures, Online First 1-11.*

Development of a stiffness variable MR damper with self-powered generation capability

X. J. Zhu [1], L. Deng [1], S. Sun [1], T. H. Yan [2], J.Q. Yu [3], Z. S. Ma [1, 4], W. H. Li [1]

[1] School of Mechanical, Materials, Mechatronic, and Biomedical Engineering, University of Wollongong, New South Wales 2522, Australia

[2] School of Mechanical and Electronic Engineering, China Jiliang University, Hangzhou 310018, People's Republic of China

[3] State Key Laboratory of Mechanical Transmission, Chongqing University, Chongqing 400044, People's Republic of China

[4] School of Mechanical and Electronic Engineering, Beijing Jiaotong University, Beijing 100044, People's Republic of China

Corresponding authors: ssun@uow.edu.au

Abstract

This paper reports a compact stiffness controllable magnetorheological (MR) damper with a self-powering capacity. Firstly, the structure, working mechanism and analysis of the damper are presented. After the prototype of the MR damper, experimental tests were conducted to evaluate its stiffness variable feature and self-powered generation capability using a hydraulic Instron test system. The testing results demonstrate that its stiffness variation range can reach 70.4% when the applied current increases from 0A to 2A.The energy generating capability of the MR damper was also evaluated using the Instron testing system under a harmonic excitation with 0.15Hz frequency and 30mm displacement. The testing results illustrate that the self-powered generation component can generate 2.595 W effective power, which is enough to control the MR component of the damper. The successful development, theoretical analysis and experimental testing of this new variable stiffness self-powered MR damper make the concept of energy free stiffness variable MR damper feasible.

Key words: Variable stiffness; Self-powered capability; MR damper.

1. Introduction

Vehicle suspension system supports the whole weight of the vehicle, provides the capability of directional control during manoeuvring and is also responsible for reducing the vibration generated by the road disturbances. Therefore, suspension of vehicle is a key component and has great influence on the performance of vehicle. Currently, passive damper has been widely utilized in suspension system for vibration reduction. The performance of the passive damper, however, is limited because it cannot adapt its parameters according to different requirements. Semi-active and active devices have been considered as new methods to advance the suspension performance. Although active suspension generally provide better ride comfort than semi-active can, its limitations of high energy consumption, potential instability, complex component requirement and control algorithm reduce its popularity [1-4]. In contrast, the semi-active vehicle suspension only requires low energy consumption, costs much less, and can provide comparable performance with active suspension. Therefore, more interest has recently been given to the semi-active suspension [5-7] and it has been considered as high-end intelligent suspension to improve the ride comfort and handling of vehicles.

Magnetorheological (MR) fluid, as a smart material, has been widely applied in vehicle industry. The rheological characteristics of MR fluid can be reversibly controlled by external magnetic field [8-11] and its response speed is very quick, i.e. within several million seconds [12, 13]. Therefore, MR fluid has been widely used as the working liquid to build MR damper, which has become one of the most promising components for semi-active vehicle suspensions in recent years [14-16], compared with the others smart materials such as electrorheological (ER) materials [17-19] . Although the energy consumption of MR damper is small, external power is still needed to control its dynamic performance, which increases the risk of the damper instability and operation cost[20]. Hence, much research has been conducted to investigate MR dampers with self-powered capability to overcome this drawback. For example, Cho et al. designed a new MR damper integrated with an electromagnetic induction (EMI) part, which has better performance than conventional systems[21, 22]. Sapinski designed an MR damper with energy harvesting capability. A linear electromagnetic generator was installed at the end of the MR damper to harvest vibration energy as well as self-sense the vibration signal [23]. Deng et al. presented an inventive philosophy for energy generators, which

was based on nonlinear vibration, and provided a method of poly-stable vibrational power generation[24]. He also developed a semi-active suspension with non-piston MR damper to reduce the vibration of a washing machine, which is a typical variable mass system[25]. Wang et al. designed a semi-active MR damper with energy regeneration function, composing of a linear DC generator, a controllable MR damper, a control circuit and a rack–pinion mechanism, for the application of elevated highways. Its improved performance was verified by numerical evaluation [26]. Deng et al. presented a stiffness variable MR damper recently, whose damping and stiffness were controllable[27]. Guan et al. proposed a new compact MR damper with self-powered capability, consisting of a conventional linear double-ended MR damper and a power generation component. The power generation part employed ball-screw mechanism and a rotary DC generator to convert mechanical vibration into electrical power [28]. However, most of the current self-powered MR dampers can only control their damping force. Another promising self-powered MR damper with variable stiffness characteristics has rarely been investigated.

Comparing with the damping controllability, the stiffness controllability can control the natural frequency of the vehicle to avoid vibration resonance. In addition, suspension stiffness controllable can also overcome the suspension stiffness design conflict because soft stiffness is required to achieve a good ride comfort and the handling stability and off-road drive of vehicles need hard suspension stiffness. As a result the stiffness controllable suspension with self-powering function is a promising method to further improve the vehicle performance. Several research have been done to control the stiffness of the suspension. Youn et al. designed a stiffness-variable suspension with a controllable air spring [29]. The experimental testing results show that variable stiffness can effectively control the vibration of vehicle. However, it requires an external air pump to control the air pressure of the air spring, which makes this design complex and not compact. Liu et al. developed a new system, in which two Voigt elements were connected in series to reduce the lateral vibration. However, the size limitation of this structure makes it unsuitable in real application [30]. In order to overcome these drawbacks, our group designed a compact shock absorber with variable stiffness and damping features[31, 32]. Although the structure of the two MR dampers is compact, their stroke is relatively short, which limits their applications.

In order to overcome the limitation of our previously reported stiffness variable MR damper,

this paper designed a long stroke stiffness controllable MR damper. What is more, the self-powering capability is integrated into the advanced damper and makes it energy free. The intention is to design the new damper with the following features and innovations: variable stiffness, self-powered generation capability, compact structure and large stroke. The paper is presented in the following orders. Section 2 presented the structure, working mechanism and prototype of the new damper. Section 3 analyses the new damper theoretically and establishes a modeling to predict the dynamic performance of the MR damper. Section 4 contains the experimental testing and result discussion regarding its variable stiffness feature and power generation capability. The last section draws the conclusion.

2. Design, analysis and prototype of the self-powered variable stiffness MR damper

2.1 Structural design of the new damper

A structural schematic of the proposed MR Damper is illustrated in Fig. 1. There were two main parts of the damper: variable stiffness part and self-powered generation part. Specifically it mainly consists of a hollow shaft generator, a ball screw bearing, two springs with different stiffness and an inner bypass MR damping cylinder. In the variable stiffness part, the inner bypass MR damper was installed between the upper spring with low stiffness and the bottom spring with high stiffness. Meanwhile, the shaft of the generator was fixed to the nut of the ball screw to constitute self-powered generation part, which can convert mechanical vibration to electrical energy. The shaft of the ball screw was connected with the shaft of damping unit and can move into the hollow shaft of the generator. The most innovative structural development of the MR device is that both variable stiffness feature and self-powered generation are integrated into this compact device.

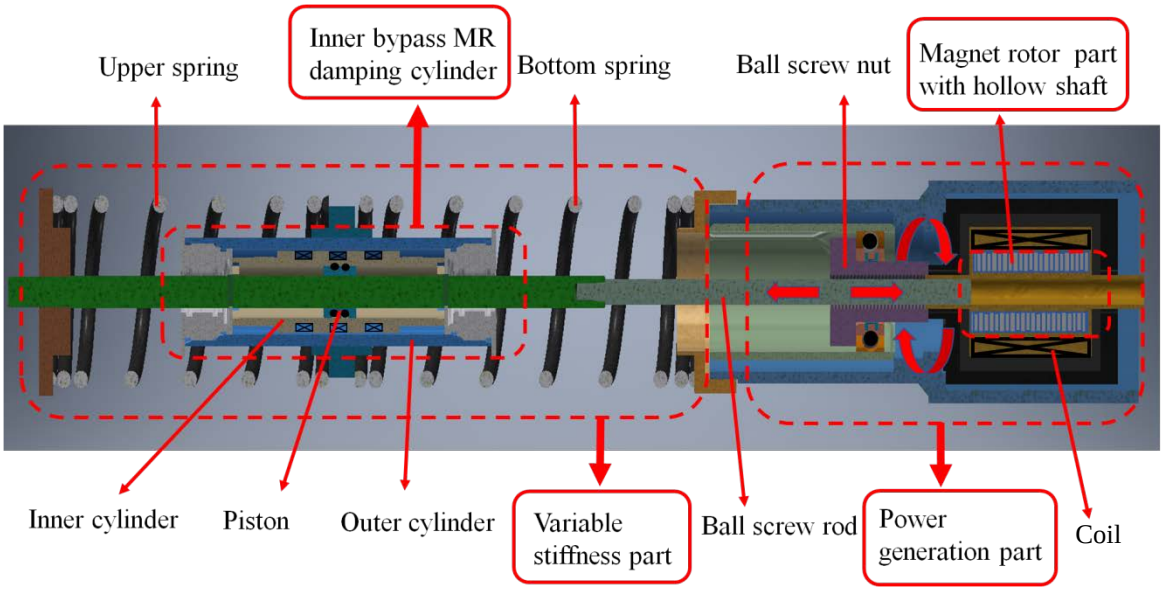

Figure 1. Structure schematic of the new damper

In order to enlarge the stroke of the damper, the MR damper's structure was designed as inner bypass type with multiple coils. The wire diameter of the coil is 0.4mm. There are 135 turns on each coil with opposite winding direction, as shown in Fig. 2 (b). Meanwhile, the hollow shaft generator could also contribute the compact structure of the new damper, allowing the ball screw rod travel through the hollow shaft. The application of the inner bypass-type MR dampers with internal coils can enlarge the stroke of the damper comparing with traditional piston structure. Specifically Fig. 2 shows a stroke comparison between the conventional stiffness MR damper we developed previously in [1] and the inner bypass stiffness controllable MR damper presented in this paper. The strokes of the two dampers can be calculated by the parameters in Table 1. The stroke of the inner bypass MR damper can reach 105 mm, which is much larger than the stroke of 71 mm of the conventional damper.

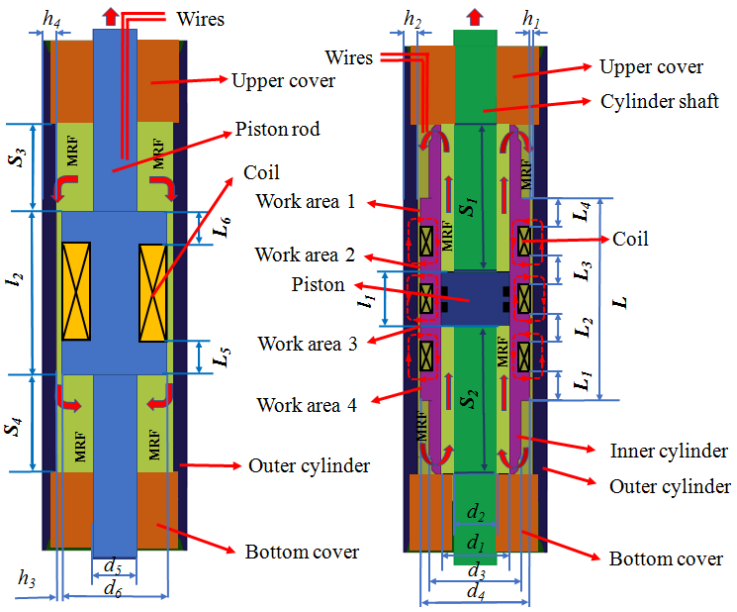

Figure 2. Schematic of the MR damping cylinder: (a) MR damper with a conventional piston [31] and (b) Inner bypass MR damper cylinder used in the new damper

Table 1. Parameters for MR damper

MRF unit parameters	Values	MRF unit parameters	Values
h_1	1mm	L_1	10mm
h_2	5mm	L_2	10mm
d_1	24mm	L_3	10mm
d_2	15mm	L_4	10mm
d_3	32mm	L	70mm
d_4	38mm	Turns of coil	135
d_5	15mm	S_1	52.5mm
d_6	30mm	S_2	52.5mm
h_3	1mm	S_3	35.5mm
h_4	4mm	S_4	35.5mm
l_1	16mm	l_2	50mm

2.2 Working principle

The overall working principle of the MR damper is that the power generated by the generator will be used to control the stiffness of the MR component so as to realize an energy free stiffness controllable suspension system.

The working principle of the variable stiffness part can be illustrated in Fig. 3, in which three different modes of the prototype are shown. For the first working mode, when the input coil current I, is zero, no magnetic field crossing MRF and the damping force will be small and allow the relative

motion between the shaft and the cylinder. In this case, the MR damper is working in Mode 1 where the bottom spring k_2 and the upper spring k_1 work in series. When the current I increases to a medium level, the device will work in Mode 2. In this case, the damping force is larger and makes the sliding motion between the damper shaft and the damping cylinder harder. The spring k_2 will be compressed more and makes the overall damper stiffness larger. Moreover, if the damping force increases to a sufficient large level and stops the relative motion between the shaft and the cylinder, the MR damper will be working in Mode 3, because only the bottom spring k_2 will be deformed under external force compression. In conclusion, the stiffness of the new damper can be controlled in the range of the minimum value of $\frac{k_1 k_2}{k_1+k_2}$ and the maximum stiffness of the bottom spring k_2. In the new MR damper, the stiffness parameters of the two springs are k_1=30220 N/m and k_2=34000 N/m.

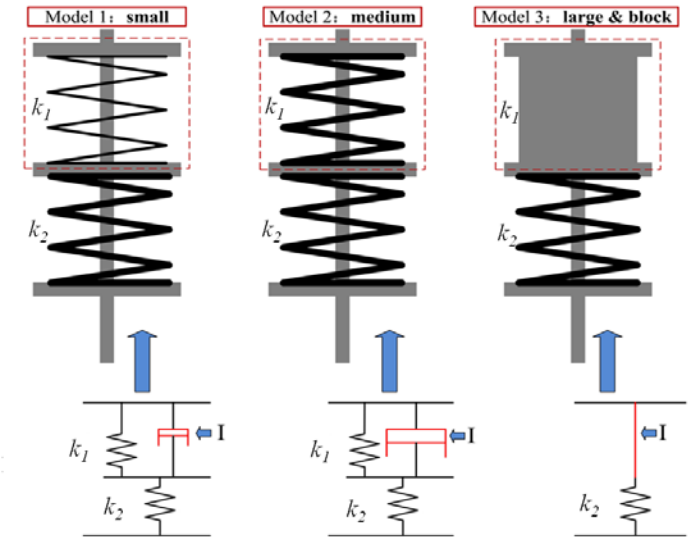

Figure 3. Working principle of the stiffness variation

The working principles of the power generation part as well as the variable stiffness MR damper are illustrated in Fig.1. Firstly, the shaft of the MR damper will move up-and-down when the upper spring k_1 was excited by the harmonic excitation. Secondly, due to the rigid connection between the shaft of the MR damper and the rod of the ball screw bearing, the up-and-down motion of the shaft could force the rod to conduct a vertical movement without rotation. Then based on the mechanism of the ball screw bearing, the rod's vertical movement induces the rotation of the nut of the ball screw bearing. As the nut is fixed to the rotor of the generator, the magnet rotor will rotate and generate energy.

2.2 Prototype of the new damper

Fig. 4 shows the prototype of the new damper, which has been manufactured and assembled. In order to decrease the magnetic reluctance of the magnetic circuit, the materials of the inner cylinder and the outer cylinder are both low carbon steel, which features high magnetic conductivity. The MR fluid GH-MRF-45, produced by Bejing Hao Hua technology limited company, was used in the prototype. Meanwhile, the τ-B curve of the MR fluid is given in Appendix A.

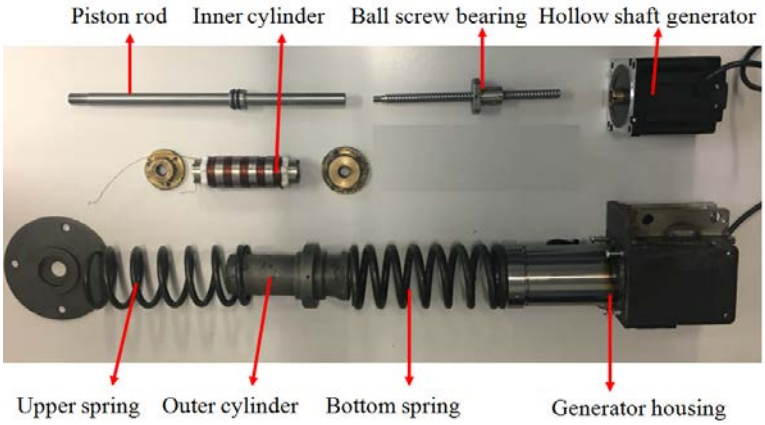

(a) Components

(b) Prototype

Figure 4 .Prototype of the new damper

3. Modelling and theoretical analysis

3.1 Modelling

According to the working principle of the MR damper, a mathematic model for the new damper is illustrated in Fig. 5. In the model, there are two parallel connected parts: variable stiffness part and power generation part. In the variable stiffness part, the controllable damping cylinder c_{mr} is parallel with the upper spring k_1 and then in a series with the bottom spring k_2. Hence, the effective stiffness of the new damper can be controlled to vary in the range of the minimum value of

$\frac{k_1 k_2}{k_1+k_2}$ and the maximum stiffness of the bottom spring k_2, when the controllable damping c_{mr} is varied by changing the current applied to the damping cylinder. In the power generation part, a generator damper c_e in parallel with a friction is used to model the force generated by the power generation part. In Fig. 5, x_2 is the stroke of the MR damper and x_1 is the compression of the bottom spring k_2.

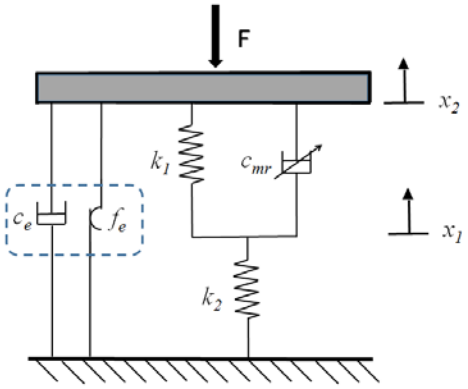

Figure 5. Mathematic model of the new damper

The equations for the model can be written as

$$F = k_2 x_1 + c_e \dot{x}_2 + f_e \tag{1}$$

where F is the force generated by the new damper; c_e and f_e are damping and friction generated by the power generation component; x_2 is the displacement of the excitation, x_1 can be determined by

$$\text{If : } F_d \geq k_2 x_1$$

$$x_1 = x_2 \tag{2}$$

$$\text{If : } F_d < k_2 x_1$$

$$F_d - k_2 x_1 + k_1 (x_2 - x_1) = 0$$

Then in order to determine F, the displacement x_1 should be calculated. As x_1 is tightly related to the damping force F_d which should be calculated to analyze the overall force of the MR damper. Fig. 2 and Table 1 show the general sizes of the MRF damping cylinder, which will be used through the calculation. The controllable force F_d is generated by the damping cylinder. The damping force can

be calculated by the following equations.

$$F_d = \Delta p * S + f_1 \tag{3}$$

where Δp is the pressure drop between the two ends of piston induced by the motion of piston; S is the effective area of piston; f_1 is the friction force generated by the friction between seal and shaft.

The pressure drop Δp can be calculated by the following equation [33]

$$\Delta p = \Delta p_\tau + \Delta p_\eta \tag{4}$$

where Δp_τ is the field-dependent pressure drop of the MRF piston and Δp_η is the viscous pressure drop.

The field-dependent pressure drop Δp_τ and viscous pressure drop Δp_η are given by equations (5) and (6), respectively.

$$\Delta p_\tau = c_1 \frac{L_1}{h_1} \tau_{y1} + c_1 \frac{L_2}{h_1} \tau_{y2} + c_1 \frac{L_3}{h_1} \tau_{y3} + c_1 \frac{L_4}{h_1} \tau_{y4} \tag{5}$$

$$\Delta p_\eta = \frac{12 \eta L q}{\pi (d_4 + h_1) {h_1}^3} \tag{6}$$

Thus the pressure drop of the piston is

$$\Delta p = c_1 \frac{L_1}{h_1} \tau_{y1} + c_1 \frac{L_2}{h_1} \tau_{y2} + c_1 \frac{L_3}{h_1} \tau_{y3} + c_1 \frac{L_4}{h_1} \tau_{y4} + \frac{12 \eta L q}{\pi (d_4 + h_1) {h_1}^3} \tag{7}$$

where $\tau_{y1}, \tau_{y2}, \tau_{y3}, \tau_{y4}$ are the yield stresses of the MR fluid under different magnetic fields of the working area1, 2, 3 and 4 respectively, as shown in Figure 2; c_1 is a coefficient, which depends on the flow velocity profile, valued between 2.0 to 5.0; η is the dynamic viscosity with no applied magnetic field, L_1, L_2, L_3, L_4 are the length of effective magnetic fields of work area 1, 2, 3, 4 respectively; q is the volume flow of MRF, L is the length of the inner cylinder's working part. h_1 is the thickness of fluid gap. d_1 is the diameter of the piston head; d_4 is the diameter of the inner cylinder's working part. The detailed values of the above parameters are illustrated in Fig. 2 and Table 1.

The volume flow of MRF can be calculated by:

$$q = \frac{\pi v(d_1^2 - d_2^2)}{4} \tag{8}$$

where the v is the velocity of piston; d_2 is the diameter of piston rod.

The effective area of piston head is expressed as:

$$S = \frac{\pi(d_1^2 - d_2^2)}{4} \tag{9}$$

Thus the damping force:

$$F_D = \frac{c_1\pi(d_1^2 - d_2^2)}{4h_1}(L_1\tau_{y1} + L_2\tau_{y2} + L_3\tau_{y3} + L_4\tau_{y4})sgn(v) + \frac{3\eta L\pi(d_1^2 - d_2^2)^2 v}{4(d_4 + h_1){h_1}^3} + f_1 \tag{10}$$

3.2 Magnetic field simulation

In order to complete the damping force calculation in Eqn. 10, the magnetic flux density across MRF should be calculated to determine the yield stress of the MRF under different current. The finite element method is applied in this section to analyze the magnetic field of the inner bypass MR damper and obtain the values of the magnetic flux density in the four activation regions under different current. Since the MR damper is a symmetrical structure, the magnetic field intensity of these four activation regions (Work Area 1, 2, 3 & 4) are symmetrical as well, as shown in Figure 6. The results of the magnetic flux density of work area 1 and Work area 4 are the same as well as the magnetic flux density of work area 2 and work area 3.

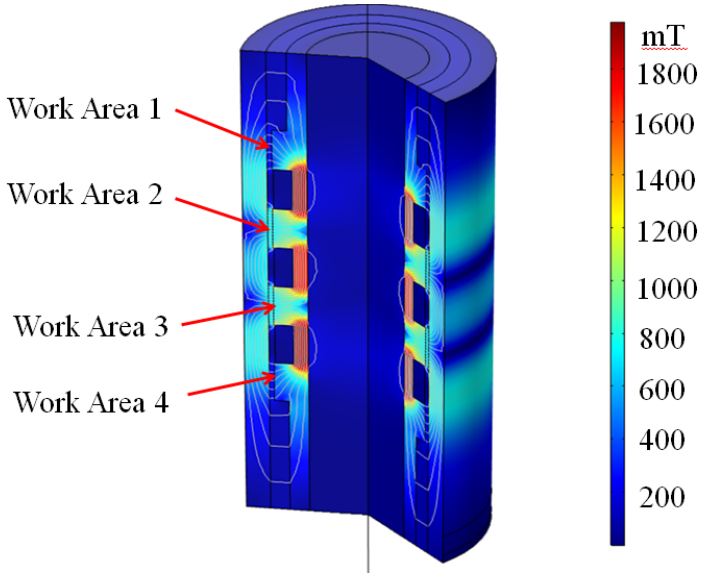

Figure 6 Magnetic field simulation

Fig. 6 presents the average flux through the four activation regions all increase with the 0.1A increment of input current *I*, which was set from 0A to 2A. The peak values of the magnetic flux density in the work area 1 and work area 2 are 260.8mT and 689.6mT respectively. In the multistage-coil structure of the MR damper, due to the additional coils that create additional magnetic flux within the same cross-sectional geometry, the average magnetic flux density in activation regions of work area 2 and work area 3 are dramatically larger than that in activation regions work area 1 and work area 4.

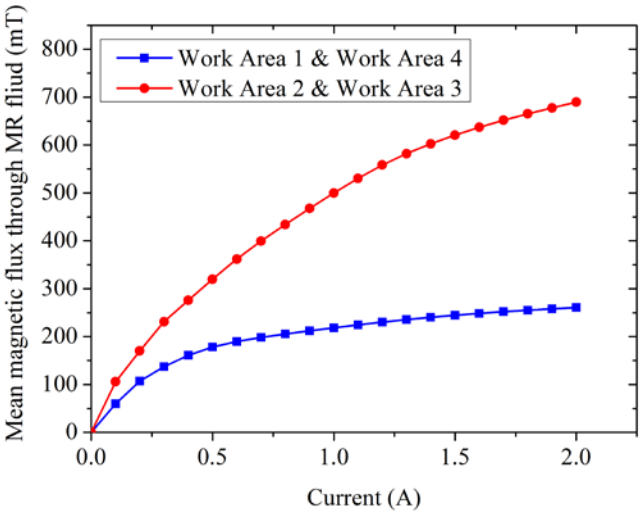

Figure 6. Average flux density through activation regions of the innovative MR damper

4. Experimental testing and result discussion

4.1 Experimental setup

In this section, experimental testing was conducted using a computer-controlled INSTRON test system (model 8033), as illustrated in Fig. 7, to demonstrate the dynamic performance of the new damper. There are three parts of the test system: the hydraulic grip, the self-powered variable stiffness MR damper and the hydraulic actuator. The hydraulic grip can fasten the top part of the MR damper and use the embedded sensors to collect the testing stroke and the generated force, meanwhile the hydraulic actuator can also grab the bottom of the damper and provide the controllable harmonic excitation to the MR damper. The tests to investigate the variable stiffness feature and the self-power generation capacity of the MR damper were conducted separately and detailed in the following two sub-sections.

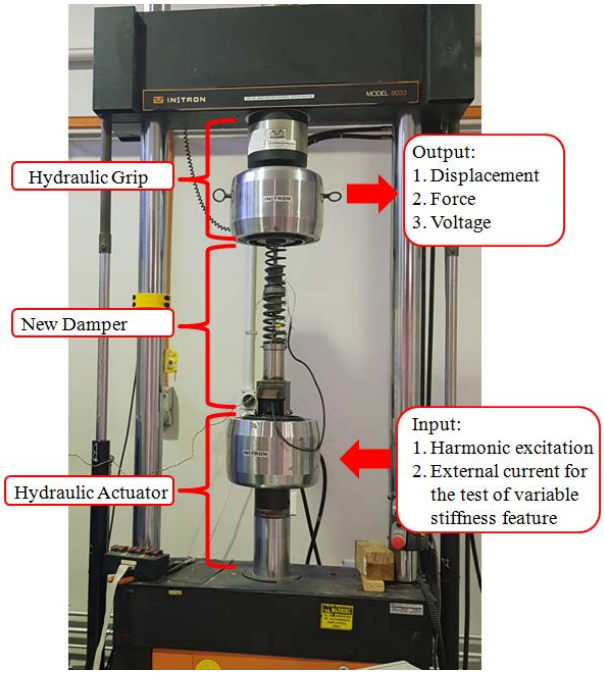

Figure 7. Instron test system installed with the prototype

4.2 Stiffness testing

The stiffness variation characteristic of the MR damper is tested systematically in this section. The self-powering element remains to be open circuit during the test. The excitation current *I* controlling the MR damping cylinder was set as 0A, 1A and 2A to control the MR damper. Meanwhile the harmonic excitation of the Instron machine is set with 0.15 Hz frequency and 20mm displacement. The testing results are presented in Fig. 8. It can be seen that the increase of the excitation current *I* leads to the increase of the effective stiffness. Similar results can be obtained under harmonic excitation with 0.15Hz frequency and 30 mm amplitude, as shown in Fig.9. The effective stiffness of the MR damper under different currents and excitation amplitudes is also calculated and plot in Fig.10. According to Fig. 10, the effective stiffness of the MR damper increases from 17.6N/mm to 25.93N/mm and 30N/mm respectively when the input current *I* increases from 0A to 1A and 2A under the harmonic excitation with 30mm amplitude. In summary, the test results verify that the damper stiffness can be controlled by external controlling current. The relative stiffness increase reaches 55.8% and 70.4% under harmonic excitation of 20mm displacement and 30mm displacement respectively, as showed in Fig. 10.

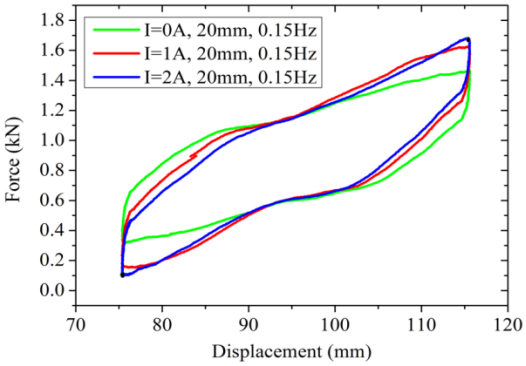

Figure 8. Force-displacement loops (20 mm)

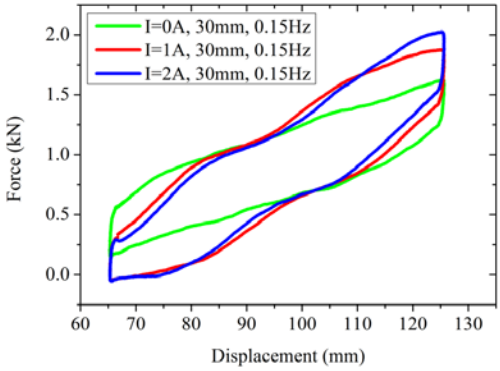

Figure 9. Force-displacement loops (30 mm)

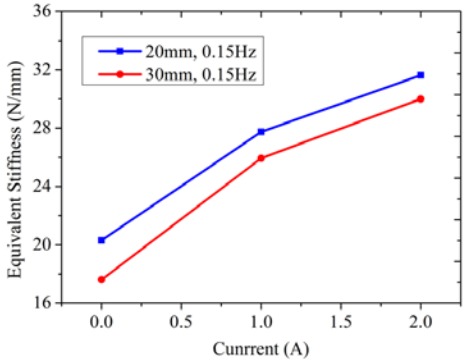

Figure 10. Equivalent stiffness of the damper

The force-velocity relationship is another important indicator to evaluate a vehicle damper. The force-velocity loops with different excitation current under different excitation amplitude are presented in Fig. 11 and Fig. 12. It is seen that the increase of input current *I* can enlarge the damping under different operation speed. The equivalent damping of the new damper can also be calculated by Eqn. 11 [34]. According to the calculation, the excitation current affect the damping the MR damper. Specifically, the max equivalent damping coefficient and the min equivalent damping coefficient of the damper under different current were calculated as 18.68kNs/m and 11.78kNs/m respectively.

$$c_{eq} = \frac{EDC}{2\pi^2 f A^2} \tag{11}$$

where c_{eq} is the equivalent damping coefficient. *EDC* is the energy dissipated per cycle, being the enclosed area of each force-displacement loop, f is the frequency of the harmonic excitation and A is the amplitude of the harmonic excitation.

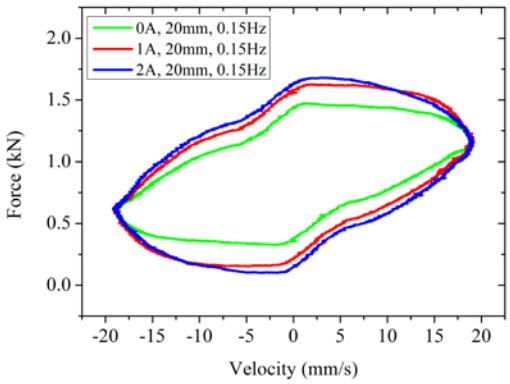

Figure 11. Force-velocity loops under 20mm amplitude

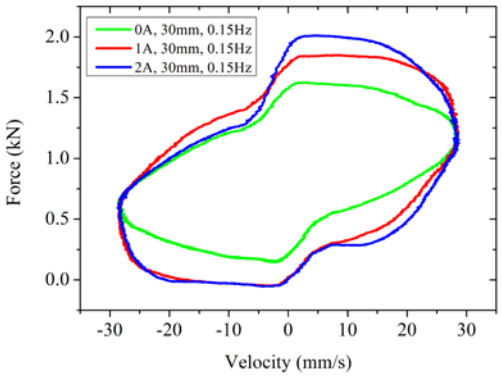

Figure 12. Force-velocity loops under 30mm amplitude

In order to verify the accuracy of the model built in section 3, the experimental data and the model simulation results under harmonic excitation of 20mm amplitude and 0.15Hz frequency are compared, as shown in Fig.13. From the comparison results it can be seen that the proposed model can predict the dynamic performance of the MR damper fairly well.

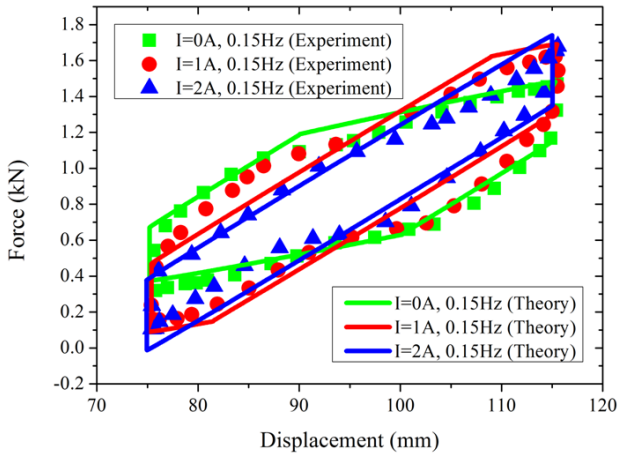

Figure 13. Comparison between the experimental results and simulation results

4.3 Testing of the self-powered generation capability

The self-powered generation capability of the MR damper was tested with an open electrical circuit firstly. The Instron machine is used to conduct this test and three excitations were set to be harmonic excitations with amplitudes of 10mm, 20mm and 30mm respectively with the same frequency of 0.15Hz. The generated voltages in the time domain under the three harmonic excitations are presented in Fig. 14 a-c. From this figure it can be seen that the generated voltage increases with the increase of the excitation amplitude. V_{rms} produced by the MR damper under the

three harmonic excitations could also be calculated, which are 1.38V, 2.94V and 4.2V, respectively [35]:

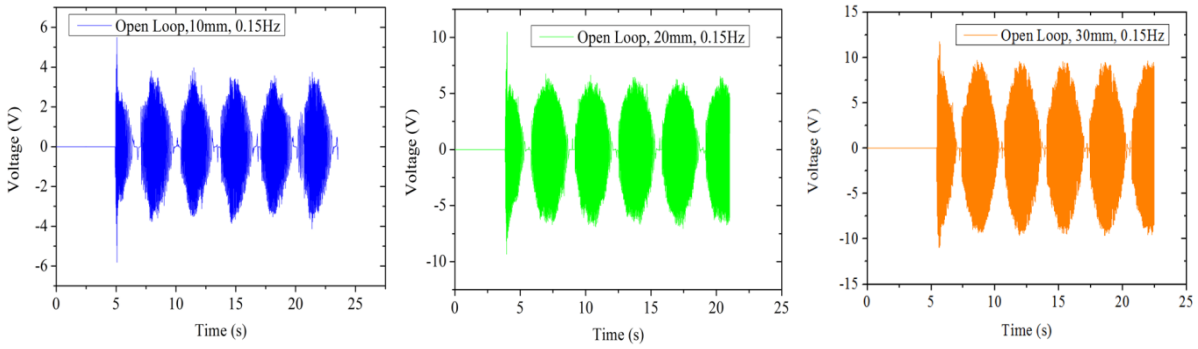

(a) (b) (c)

Figure 14. Generated voltage with open circuit (a) 10mm amplitude (b) 20mm amplitude (c) 30mm amplitude

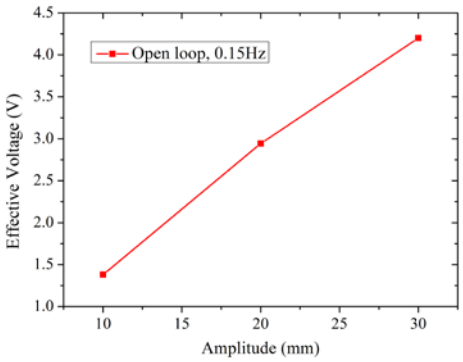

Figure 15. Effective voltages with open circuit

As the second step to evaluate the self-powering capability of the MR damper, its power generation component was evaluated with a closed electrical circuit. The bypass cylinder's coil of the MR damper served as an electrical load. The testing condition is set to be harmonic excitation with 30mm amplitude and 0.15Hz frequency and the resistance value of the MR damper is 6.2 Ω. The testing results are illustrated in Fig.16, 17, 18, 19 and 20. Ignoring the transient voltage and power at the beginning, the maximum voltage V_{max} can reach 10V while the maximum power can reach 14W at the Steady state. The effective power and the RMS of voltage, V_{rms}, under closed loop test can be calculated, which can reach 2.595 W and 4.011V, respectively.

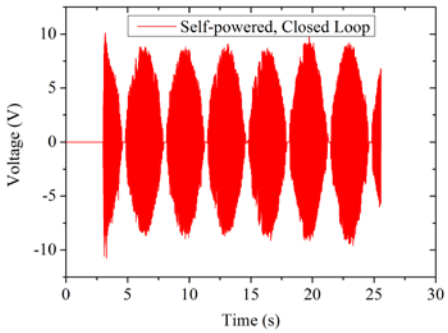

Figure 16. The generated voltage (closed circuit)

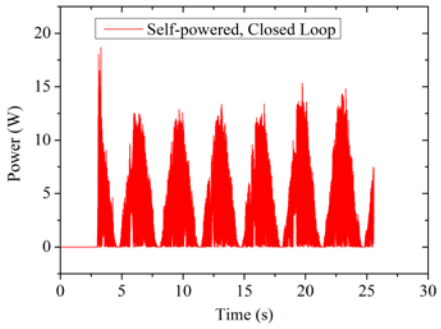

Figure 17. The generated power (closed circuit)

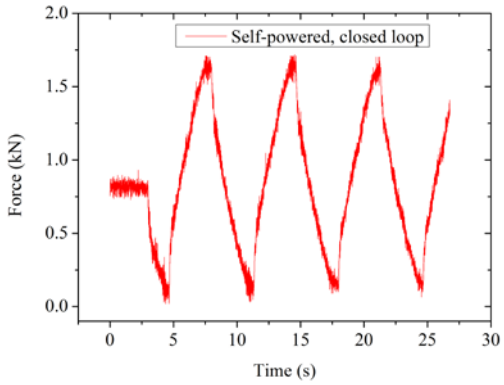

Figure 18. The damper force (closed circuit)

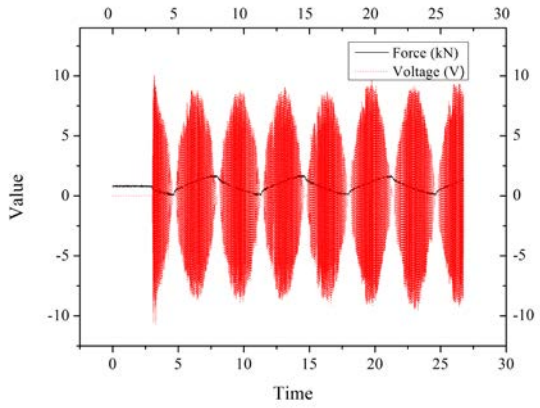

Figure 19 The comparison of force and voltage in time domain

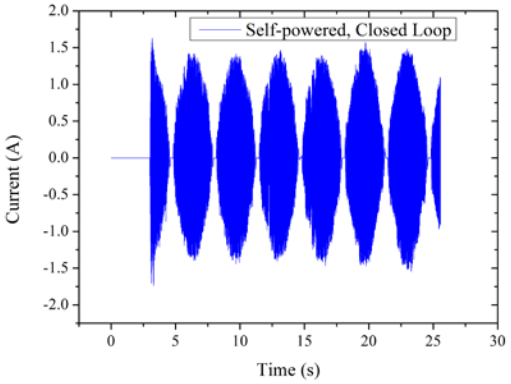

Figure 20. The generated current (closed circuit)

5 Conclusion

This paper successfully developed a compact energy free MR vehicle damper whose stiffness is controllable. The stiffness variation mechanism of the new damper was theoretically analyzed. Experimental testing was conducted to evaluate the performance of the MR damper. The stiffness

controllability testing demonstrates that the stiffness of the MR damper can vary 70.4% when the applied current increases from 0A to 2A under the harmonic excitation of 0.15Hz frequency and 30mm amplitude. The evaluation results of the self-powering component verify that the effective energy generated by the MR damper reaches to 2.595 W, which is sufficient to control its MR component.

Acknowledges

This research is supported by ARC Linkage Grant (LP150100040).

REFERENCES

[1] S. Sun, X. Tang, W. Li, and H. Du, "Advanced vehicle suspension with variable stiffness and damping MR damper," in *Mechatronics (ICM), 2017 IEEE International Conference on*, 2017, pp. 444-448: IEEE.

[2] G. Priyandoko, M. Mailah, and H. Jamaluddin, "Vehicle active suspension system using skyhook adaptive neuro active force control," *Mechanical systems and signal processing,* vol. 23, no. 3, pp. 855-868, 2009.

[3] M. Jonasson and F. Roos, "Design and evaluation of an active electromechanical wheel suspension system," *Mechatronics,* vol. 18, no. 4, pp. 218-230, 2008.

[4] K.-G. Sung, Y.-M. Han, J.-W. Cho, and S.-B. Choi, "Vibration control of vehicle ER suspension system using fuzzy moving sliding mode controller," *Journal of Sound and Vibration,* vol. 311, no. 3-5, pp. 1004-1019, 2008.

[5] X. Tang, H. Du, S. Sun, D. Ning, Z. Xing, and W. Li, "Takagi–Sugeno fuzzy control for semi-active vehicle suspension with a magnetorheological damper and experimental validation," *IEEE/ASME Transactions on Mechatronics,* vol. 22, no. 1, pp. 291-300, 2017.

[6] U. Solomon and C. Padmanabhan, "Semi-active hydro-gas suspension system for a tracked vehicle," *Journal of Terramechanics,* vol. 48, no. 3, pp. 225-239, 2011.

[7] T. Gordon, "Non-linear optimal control of a semi-active vehicle suspension system," *Chaos, Solitons & Fractals,* vol. 5, no. 9, pp. 1603-1617, 1995.

[8] S.-W. Cho, H.-J. Jung, and I.-W. Lee, "Smart passive system based on magnetorheological damper," *Smart Materials and Structures,* vol. 14, no. 4, p. 707, 2005.

[9] H. Wang, A. Tian, Q. Tang, Z. Chen, and B. Liu, "Research on rheological property of magnetorheological fluid," in *3rd International Symposium on Advanced Optical Manufacturing and Testing Technologies: Advanced Optical Manufacturing Technologies*, 2007, vol. 6722, p. 672230: International Society for Optics and Photonics.

[10] P. Kuzhir, M. López-López, and G. Bossis, "Abrupt contraction flow of magnetorheological fluids," *Physics of Fluids,* vol. 21, no. 5, p. 053101, 2009.

[11] C. Miao, K. M. Bristol, A. E. Marino, S. N. Shafrir, J. E. DeGroote, and S. D. Jacobs, "Magnetorheological fluid template for basic studies of mechanical-chemical effects during polishing," in *Optical Manufacturing and Testing VII*, 2007, vol. 6671, p. 667110: International Society for Optics and Photonics.

[12] J. D. Carlson and M. R. Jolly, "MR fluid, foam and elastomer devices," *Mechatronics,* vol. 10, no. 4, pp. 555-569, 2000.

[13] J. D. Carlson, "Critical factors for MR fluids in vehicle systems," *International Journal of Vehicle Design,* vol. 33, no. 1-3, pp. 207-217, 2003.

[14] G. Tsampardoukas, C. W. Stammers, and E. Guglielmino, "Hybrid balance control of a magnetorheological truck suspension," *Journal of Sound and Vibration,* vol. 317, no. 3-5, pp. 514-536, 2008.

[15] M. Yu, X. Dong, S. B. Choi, and C. Liao, "Human simulated intelligent control of vehicle suspension system with MR dampers," *Journal of sound and vibration,* vol. 319, no. 3, pp. 753-767, 2009.

[16] J. N. Potter, S. A. Neild, and D. J. Wagg, "Quasi-active suspension design using magnetorheological dampers," *Journal of sound and vibration,* vol. 330, no. 10, pp. 2201-2219, 2011.

[17] P. Chen, Q. Cheng, L.-M. Wang, Y. D. Liu, and H. J. Choi, "Fabrication of dual-coated graphene oxide nanosheets by polypyrrole and poly (ionic liquid) and their enhanced electrorheological responses," *Journal of Industrial and Engineering Chemistry,* vol. 69, pp. 106-115, 2019.

[18] T. Tian and M. Nakano, "Fabrication and characterisation of anisotropic magnetorheological elastomer with 45° iron particle alignment at various silicone oil concentrations," *Journal of Intelligent Material Systems and Structures,* vol. 29, no. 2, pp. 151-159, 2018.

[19] Y. Tong, X. Dong, and M. Qi, "Improved tunable range of the field-induced storage modulus by using flower-like particles as the active phase of magnetorheological elastomers," *Soft matter,* vol. 14, no. 18, pp. 3504-3509, 2018.

[20] X. Dong, "Design and characterization of axial flux permanent magnet energy harvester for vehicle magnetorheological damper," *Smart Materials and Structures,* vol. 25, no. 1, p. 015024, 2015.

[21] B. Sapiński, "Experimental study of a self-powered and sensing MR-damper-based vibration control system," *Smart Materials and Structures,* vol. 20, no. 10, pp. 105007-105019, 2011.

[22] K.-M. Choi, H.-J. Jung, H.-J. Lee, and S.-W. Cho, "Feasibility study of an MR damper-based smart passive control system employing an electromagnetic induction device," *Smart Materials and Structures,* vol. 16, no. 6, p. 2323, 2007.

[23] B. Sapiński, "Energy-harvesting linear MR damper: prototyping and testing," *Smart Materials and Structures,* vol. 23, no. 3, p. 035021, 2014.

[24] H. Deng *et al.*, "Poly-stable energy harvesting based on synergetic multistable vibration," *Communications Physics,* vol. 2, no. 1, p. 21, 2019.

[25] H. Deng *et al.*, "Development of a non-piston MR suspension rod for variable mass systems," *Smart Materials and Structures,* vol. 27, no. 6, p. 065014, 2018.

[26] Z. Wang, Z. Chen, and B. F. Spencer, "Self-powered and sensing control system based on MR damper: presentation and application," in *Sensors and Smart Structures Technologies for Civil, Mechanical, and Aerospace Systems 2009*, 2009, vol. 7292, p. 729240: International Society for Optics and Photonics.

[27] H. Deng *et al.*, "Variable stiffness mechanisms of dual parameters changing magnetorheological fluid devices," *Smart Materials and Structures,* vol. 26, no. 12, p. 125014, 2017.

[28] G. Xinchun, H. Yonghu, R. Yi, L. Hui, and O. Jinping, "A novel self-powered MR damper: theoretical and experimental analysis," *Smart Materials and Structures,* vol. 24, no. 10, p. 105033, 2015.

[29] I. Youn and A. Hać, "Semi-active suspensions with adaptive capability," *Journal of Sound and Vibration,* vol. 180, no. 3, pp. 475-492, 1995.

[30] Y. Liu, H. Matsuhisa, H. Utsuno, and J. G. Park, "Vibration isolation by a variable stiffness and damping system," *JSME International Journal Series C Mechanical Systems, Machine Elements and Manufacturing,* vol. 48, no. 2, pp. 305-310, 2005.

[31] S. Sun, J. Yang, W. Li, H. Deng, H. Du, and G. Alici, "Development of a novel variable stiffness and damping magnetorheological fluid damper," *Smart Materials and Structures,* vol. 24, no. 8, p. 085021, 2015.

[32] S. Sun *et al.*, "A compact variable stiffness and damping shock absorber for vehicle suspension," *IEEE/ASME Transactions on Mechatronics,* vol. 20, no. 5, pp. 2621-2629, 2015.

[33] G. Hu, M. Long, M. Huang, and W. Li, "Design, analysis, prototyping, and experimental evaluation of an efficient double coil magnetorheological valve," *Advances in Mechanical Engineering,* vol. 6, p. 403410, 2014.

[34] Y. Li, J. Li, W. Li, and B. Samali, "Development and characterization of a magnetorheological elastomer based adaptive seismic isolator," *Smart Materials and Structures,* vol. 22, no. 3, p. 035005, 2013.

[35] M. Kampik, H. Laiz, and M. Klonz, "Comparison of three accurate methods to measure AC voltage at low frequencies," *IEEE Transactions on instrumentation and measurement,* vol. 49, no. 2, pp. 429-433, 2000.

Appendix A: The material property of the MRF used in this paper

The τ-B relationship of the MRF used in this paper is given in Figure 16. By fitting the τ-B curve of MRF, the relationship between the shear yield stress and the applied magnetic flux density can be expressed as

$$\tau_B = -62.47B^4 + 64.76B^3 + 53.40B^2 + 11.32B + 0.09547 \quad (14)$$

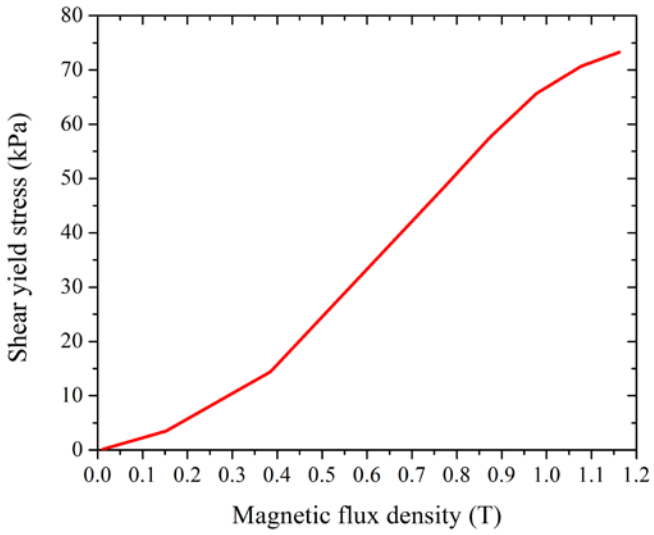

Figure 16. τ-B curve